

Cooperative Channel Modeling

Mischa Dohler

30 September 2009

CTTC, Barcelona

– Lecture Outline –

1. **General Channel Characteristics**

- (a) Propagation Principles
- (b) Propagation Modeling
- (c) Fading

2. **Regenerative Relaying Channel**

- (a) Quick Intro
- (b) Pathloss Modeling
- (c) Shadowing Modeling
- (d) Fading Modeling
- (e) Fading Distribution
- (f) Temporal Characteristics

3. **Transparent Relaying Channel**

4. **Concluding Remarks**

PART 1

General Channel Characteristics

– Propagation Scenario –

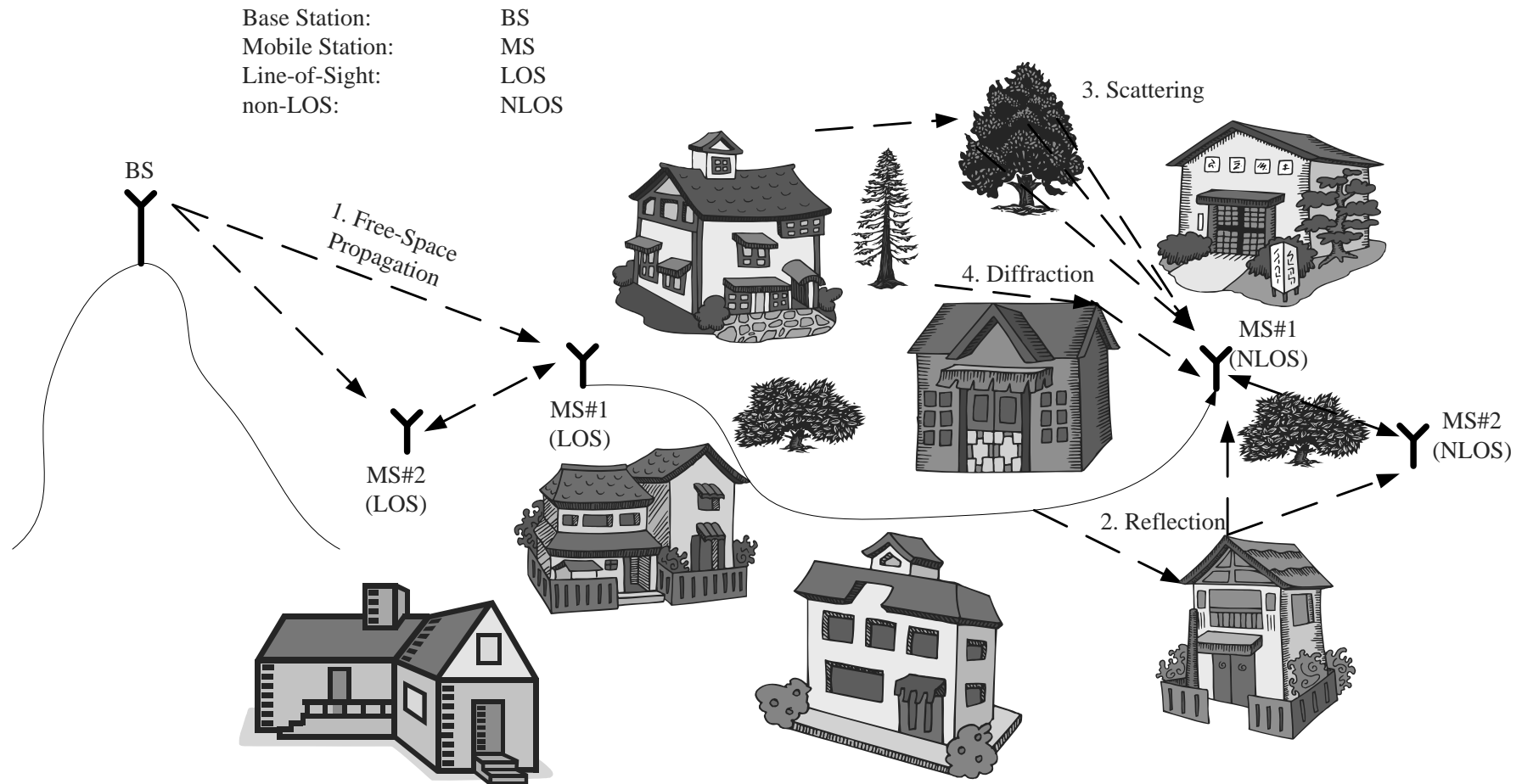


Figure 1: Channel scenario for LOS/NLOS traditional and cooperative links.

1.1 Propagation Principles

– Wave Propagation –

- **Transmitter.** The modulated signal at the transmitter is fed into a finite-length wire antenna of length l from which it decouples in form of an electromagnetic (EM) wave of wavelength λ . The efficiency of the overall radiated power is roughly proportional to $(l/\lambda)^2$.
- **Propagation.** The decoupled wave oscillates in time with angular frequency $\omega = 2\pi f = 2\pi/T$ and in space with spatial frequency $k = 2\pi/\lambda$, where f is the frequency, T the period, $\lambda = c/f$ the wavelength, and c the speed of light. It is composed of an electric component of strength E and a magnetic component H . In far field, $E = E_0 \cdot e^{j(\omega \cdot t - \mathbf{k} \cdot \mathbf{r})}$.
- **Receiver.** The clutter causes several copies of the wave to impinge upon and couple into the receive antenna, where they are again converted into an electric signal and processed by the receiver chain.

– Propagation Mechanisms –

- **Free Space Propagation.** Under the main condition that $d \gg \lambda$ and no clutter is encountered, the propagating wave undergoes free space propagation. It is a distance dependent effect which obeys Friis' transmission equation given by
$$P_r = P_t \cdot G_t \cdot G_r \cdot \lambda^2 / (4\pi d)^2.$$
- **Reflection and Refraction.** Under the condition that $\lambda \gg \Delta h$ and $s \gg \lambda$, a part of the wave reflects off the clutter's surface and the remaining part refracts into the clutter; $E_{\text{refl}} = R \cdot E_{\text{imp}}$ where R is governed by Fresnel's Law [1].
- **Scattering.** Under the condition that $\lambda \approx \Delta h$ and $s \gg \lambda$, the impinging wave is known to be scattered off the clutter's surface. The rougher the surface the stronger the impact of the scattered component which is typically assumed to be Gaussian distributed.
- **Diffraction.** Under the condition that the clutter has a few singular edges or curvatures which are of the size of λ or smaller, diffraction occurs. It essentially guarantees that an EM wave can still reach a zone shadowed by an object.

– Signal Distortions [1/2] –

- **Temporal Distortion – Doppler Effect.** The movement of transmitter and/or receiver (and/or clutter) causes the wave to be perceived at a different frequency than originally emitted, i.e. $f_{\text{perceived}} = f_{\text{original}} \cdot (1 + v/c)$, where v is the relative speed between transmitter and receiver projected onto the line connecting both. This impacts the evolution of the received signal over time.

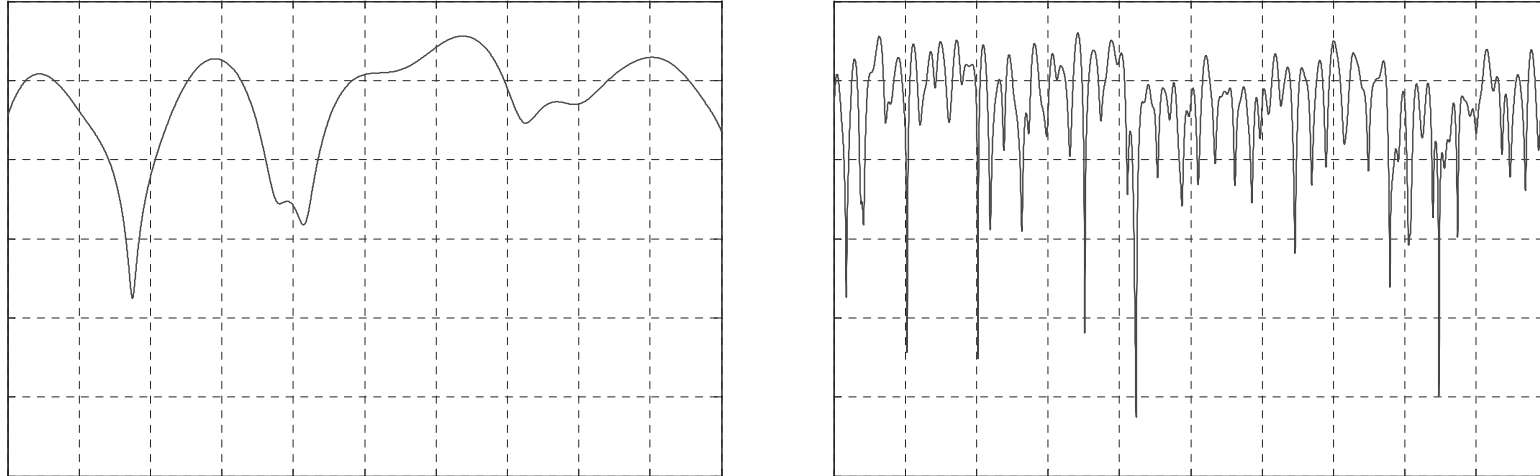
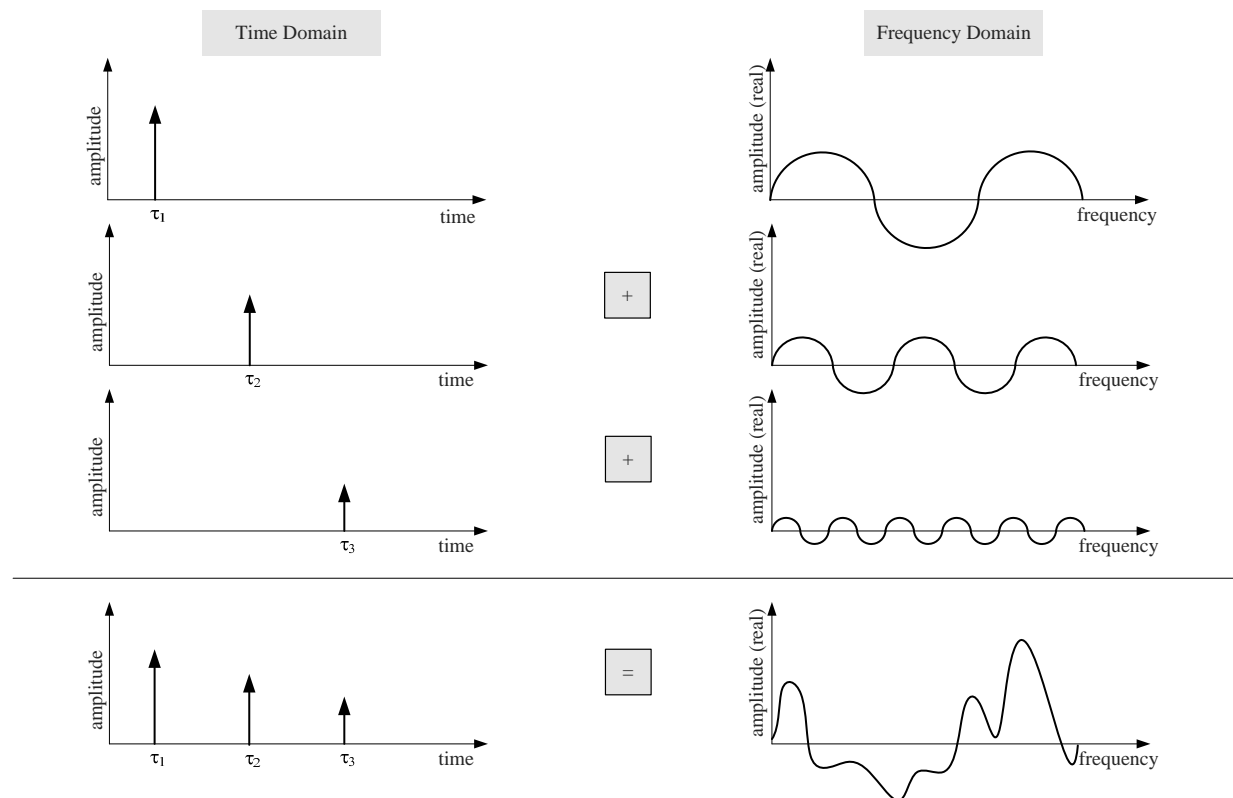


Figure 2: Field strength versus time, where little movement (left) causes only little variation and a lot of movement (right) causes more variation over the same time window of observation.

– Signal Distortions [2/2] –

- **Spectral Distortion — Multipath Propagation.** A multitude of clutter objects causes multiple waves to reach the receiver at different delays, where each of these waves will have undergone different free space propagation, reflection, etc. These multiple delayed copies are often referred to as multipath components (MPCs). The sum of these delayed signals causes selectivity in the frequency domain.



– Resulting Wireless Channel –

- **Adding It All Up.** All of the above-discussed effects can now be summarized in a single equation where the received signal is composed of the sum of the impinging MPCs, where $\sum_{\text{MPCs}} = (\text{LOS}) + \sum \text{once reflected} + \sum \text{twice reflected} + \dots$

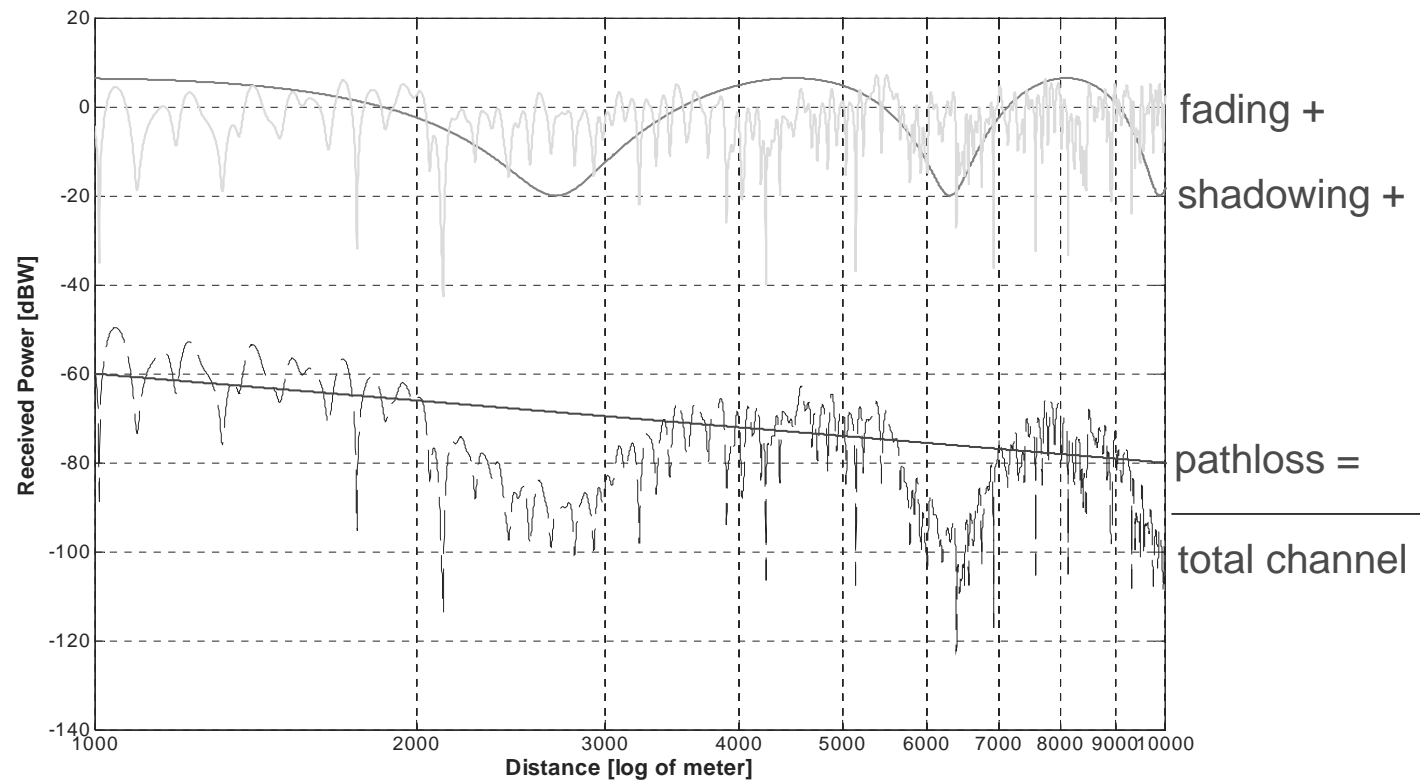


Figure 3: The sum in dB or product in linear scale of pathloss, shadowing and fading yield the actually perceived wireless channel.

1.2 Propagation Modeling

– Pathloss –

- **Free-Space Pathloss Model.** The simplest of all models, it assumes a loss of 20 dB/dec. It can be formalized as $L(d) = L(d_0) \cdot (d/d_0)^2$, where $L(d_0)$ is the power measured at some (far-field) reference distance d_0 .
- **Single-Slope Pathloss Model.** Taking the steeper decay due to clutter into account, this model assumes a loss of $10 \cdot n$ dB/dec, where n is the pathloss coefficient which can range from $n = 1.5$ (waveguides), $n = 2 \dots 4$ (LOS + clutter), $n = 4 \dots 6$ (NLOS + clutter). It can be formalized as $L(d) = L(d_0) \cdot (d/d_0)^n$. It is clearly an excellent modeling tradeoff between simplicity and accuracy.
- **Dual-Slope Pathloss Model.**
- **Deterministically Simulated Pathloss Behavior.**
- **Empirically-Fitted Pathloss Model.**
- **Real-World Measured Pathloss.**

– Shadowing –

- **Distribution.** The probability density distribution (PDF) of the received power in dB due to shadowing is given as: $p(S) = \frac{1}{\sqrt{2\pi}\sigma_{\text{dB}}} \exp \left\{ - \left(\frac{S}{\sqrt{2}\sigma_{\text{dB}}} \right)^2 \right\}$, where σ_{dB} is the standard deviation (not variance) of the shadowing process in dB (not linear scale).
- **Auto-Correlated Shadowing.** The autocorrelation shadowing coefficient, usually applied in dB, is obtained as $R(\Delta d) \triangleq \mathbb{E} \{ S(d) \cdot S(d + \Delta d) \} \propto e^{-\frac{\Delta d}{d_{\text{corr}}}}$, where d_{R} is the correlation distance which depends on the distance between Tx and Rx.
- **Cross-Correlated Shadowing.** The autocorrelation shadowing coefficient is

$$R(\Delta\phi) \triangleq \mathbb{E} \{ S(d_1) \cdot S(d_2) \} \propto \begin{cases} \sqrt{\frac{d_1}{d_2}} & \text{for } 0 \leq \Delta\phi \leq \phi_{\text{thr}} \\ \frac{\phi_{\text{thr}}}{\Delta\phi} \sqrt{\frac{d_1}{d_2}} & \text{for } \phi_{\text{thr}} < \Delta\phi \leq \pi, \end{cases} \quad (1)$$

where d_1 and d_2 are the respective distances between the MS and the BSs;

$$\phi_{\text{thr}} = 2 \arcsin(d_{\text{corr}}/(2d_1)).$$

– Fading –

- **Resolution of MPCs.** As per Figure 4, the envelope a_i and phase ϕ_i for a fixed MPC i model the unresolvable intra-symbol interference. The resolvable inter-symbol interference is modeled by different i 's at given delays τ_i .
- **Channel Impulse Response.** Fading is quantified by means of the channel's impulse response, which in simplified notation reads: $h = \sum_i a_i \cdot e^{j\phi_i} \cdot \delta(t - \tau_i)$, where h is the generally complex channel coefficient, a_i its amplitude, ϕ_i its phase and τ_i its delay.

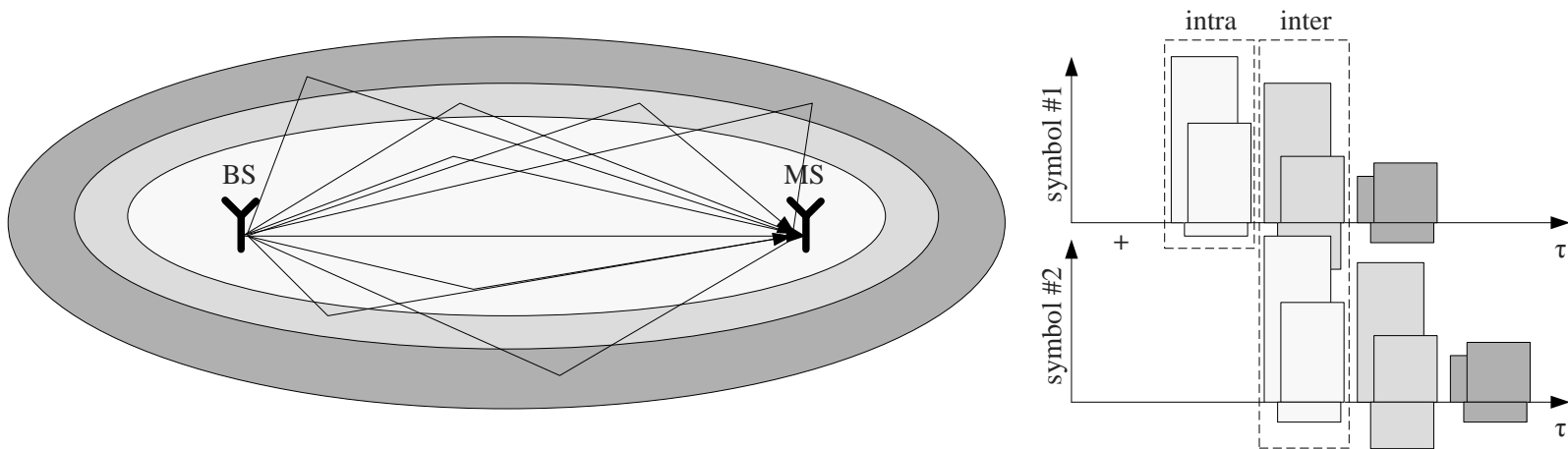


Figure 4: Origin of the intra-symbol and inter-symbol interference due to multipath propagation.

1.3 Fading

– Important Parameters –

- **Envelope** a_i . For a fixed i , the channel amplitude/envelope a_i is a random variable which is due to the random addition of many intra-symbol wave components. Different statistics of a_i have been observed which mainly depend on the operational conditions. Its envelope typically obeys Rayleigh, Ricean, Nakagami and Gamma distributions.
- **Phase** ϕ_i . The phase ϕ_i is typically but not necessarily uniformly distributed. The distribution of the phase impacts system behavior and the auto-correlation function.
- **Delay Profile** τ_i . Parameters describing the PDP are the total power gain, given as $\bar{g}_{\text{total}} = \sum_i \bar{g}_i$, the excess delay, defined as $\tau_{\text{excess}} = \tau_{\text{last resolvable tap}} - \tau_1$, the mean delay $\tau_{\text{mean}} = 1/\bar{g}_{\text{total}} \cdot \sum_i \bar{g}_i \tau_i$, and most importantly the RMS delay spread, defined as

$$\tau_{\text{RMS}} = \sqrt{\frac{\sum_i \bar{g}_i \tau_i^2}{\bar{g}_{\text{total}}} - \tau_{\text{mean}}^2}. \quad (2)$$

– Selectivity versus Non-Selectivity [1/2] –

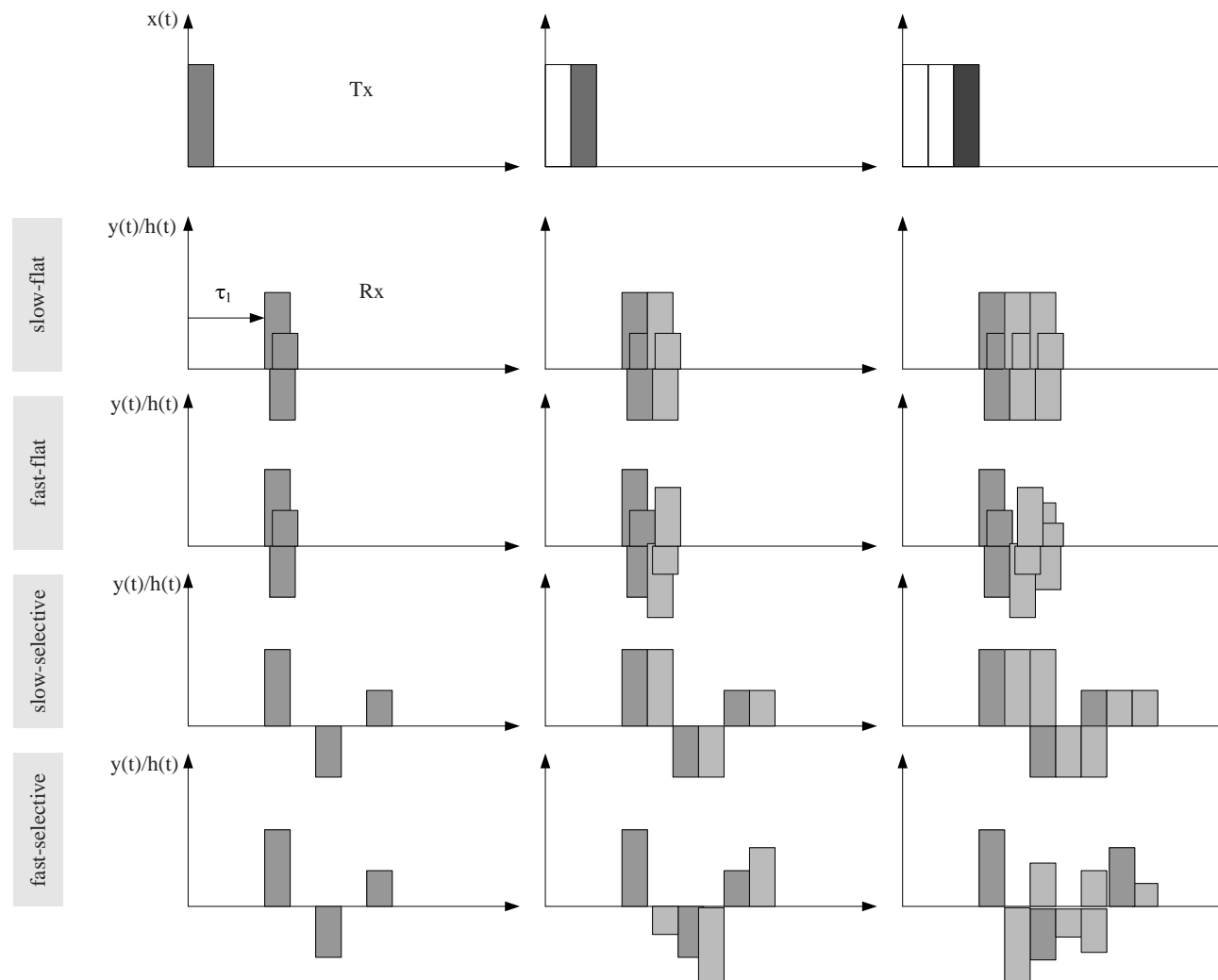


Figure 5: In respective order, the four fading cases of slow and frequency-flat, fast and frequency-flat, slow and frequency-selective, fast and frequency selective.

– Selectivity versus Non-Selectivity [2/2] –

- **Temporal Domain – Slow versus Fast Fading.** The system is said to undergo slow fading if $T_s < T_c$ and fast fading otherwise. The distinction between either has a profound impact on the choice of modulation, pilot density, etc. It is further characterized by the level crossing rate (LCR), the average fade duration (AFD), etc.
- **Spectral Domain – Flat versus Selective Fading.** The system is said to undergo flat fading if $B_s < B_c$ and frequency-selective fading otherwise. The channel is flat fading if $T_s > \tau_{\text{RMS}}$ which implies that all MPCs arrive more or less at the same time and hence only one MPC is resolved reducing the channel to $h = a \cdot e^{j\phi}$. Contrary, if $T_s < \tau_{\text{RMS}}$, more than one MPC is resolved which leads to ISI.
- **Spatial Domain – Selective versus Non-Selective Fading.** The system is said to undergo spatially non-selective fading if $d_a < d_c$ and spatially selective fading otherwise. The distinction between either has a profound impact on the performance of MIMO systems.

PART 2

Regenerative Relaying Channel

2.1 Quick Intro

– Typical Regenerative Topology –

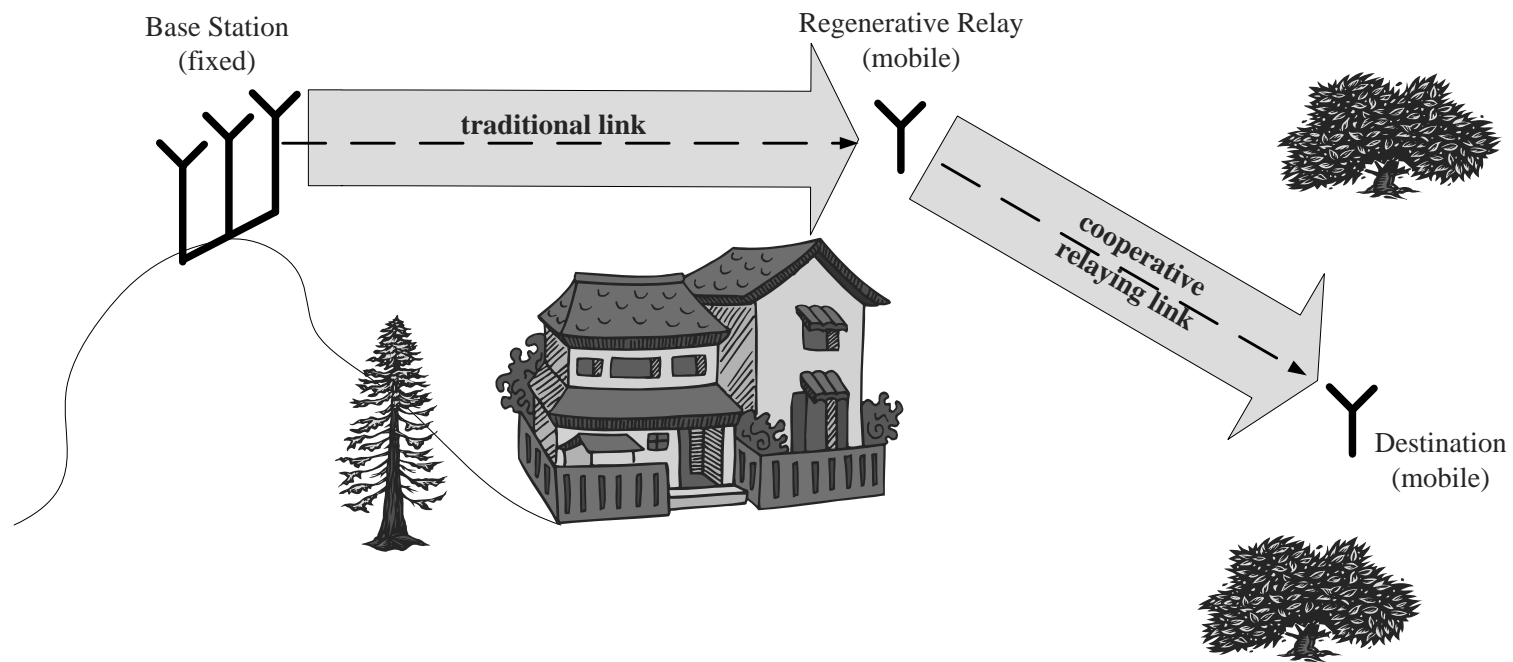


Figure 6: An example of a regenerative relaying channel.

– System Assumption –

- **Decoupling of Relay Stages.** The relay regenerates the signal which inherently decouples the fading channels before and after the relay.
- **Modeling Approach.** Unlike the transparent relay case, the channel of each segment can therefore be modeled separately which yields:

$$y_i = \sqrt{G_i} h_i x_i + n_i, \quad (3)$$

where x_i , y_i and n_i are respectively the transmitted signal, the received signal and the additive white Gaussian noise (AWGN) with power σ_i^2 experienced in the i –th relaying segment. Furthermore, $G_i = L_i \cdot S_i$ is the large-scale channel gain due to pathloss and shadowing and h_i is the generally complex channel coefficient due to fading.

- **Parametric Characterization.** The wireless regenerative relaying channel is hence characterized in each segment separately by L_i , S_i and h_i where the impact of each of these factors will be subsequently discussed.

– Key Channel Parameters –

- **Pathloss.** The pathloss coefficient of the traditional link varies between $n < 2$ in e.g. wave guiding streets, $n = 2$ (LOS) and $n = 2, \dots, 4$ (NLOS) and the segment of a cooperative link exhibits coefficients from $n = 2$ (LOS) to $n = 4, \dots, 6$ (NLOS). Clearly, the increased amount of clutter at both ends yields a larger average pathloss.
- **Shadowing.** Both traditional and cooperative links suffer from lognormal shadowing with the traditional link exhibiting a standard deviation σ_{dB} of $2, \dots, 6$ dB (LOS) and $6, \dots, 18$ dB (NLOS), whereas the cooperative link is in the range of $0, \dots, 2$ dB (LOS) and $2, \dots, 10$ dB (NLOS).
- **Fading.** Whilst the class of fading distributions does not change for the cooperative link, the first and second order ordinary and joint moments may change. The reason why the class of distributions does not change is because the relay segments are decoupled and each segment obeys the same propagation principles. The reason why the moments change is because the amount of clutter changes, its distribution, etc.

– Impact on End-to-End Performance –

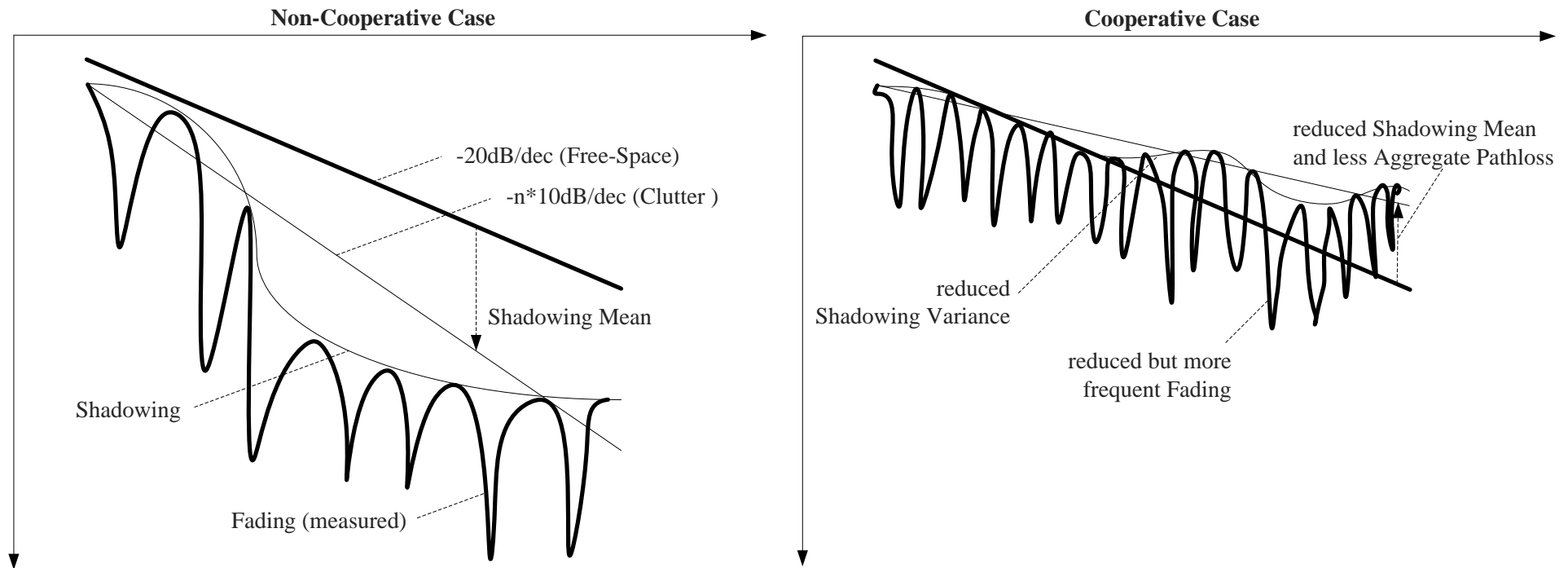


Figure 7: Regenerative cooperative communication impacts fading and shadowing and generally reduces pathloss.

2.2 Pathloss Modeling

– Change of Breakpoint Distance –

- **Traditional Breakpoint.** Most pathloss models exhibit a breakpoint behavior. The breakpoint distance can in some settings be approximately calculated as

$$d_{\text{bp}} \approx 4h_{\text{t}}h_{\text{r}}/\lambda,$$

where h_{t} and h_{r} are the transmitter and receiver heights respectively.

- **Reduced Breakpoint Distance.** Compared to BS-MS, reducing the antenna height of MS-MS by an order of magnitude (e.g. from 20m to 2m), the breakpoint distance is also reduced by an order of magnitude (e.g. from 100 m to 10 m).
- **System Impact.** Placing a relay between BS and some MS may advantageously move the traditional link from beyond the breakpoint to before the breakpoint but will likely cause the cooperative relaying link to be beyond breakpoint distance.

– Aggregate Pathloss Powergains [1/2] –

- **Nonlinear Pathloss Behavior.** Pathloss versus distance is highly non-linear, facilitating significant aggregate power gains. Therefore, placing relays in-between source and destination yields significant gains.
- **Example Topology.** Let us e.g. assume a system with the source and destination separated by d meters and relays placed at equidistance between them so that N relay segments occur. Assuming then an example pathloss model from [2], the pathloss in each relaying segment can be calculated in decibel as follows:

$$L = b + 10n \log_{10}(d/N), \quad (4)$$

where b is a constant and n the pathloss coefficient.

– Aggregate Pathloss Powergains [2/2] –

- **Aggregate Pathloss Powergains.** The aggregate power gains due to this non-linear pathloss behavior, calculated as $10 \log_{10} N + L$, is summarized in Table 1 w.r.t. the case without relay in percent and in absolute dB values, assuming $d = 500$ m, $b = -62.01$ dB and $n = 5.86$.
- **General Trend.** These gains are significant which can be attributed to the large pathloss coefficient n . Furthermore, these gains even increase if a dual-slope pathloss model is assumed.

Relay Segments	1	2	3	4	5	6	7	8	9	10
Relative Gain [%]	0	18	32	44	55	65	75	84	93	102
Absolute Gain [dB]	0	15	23	29	34	38	41	44	46	49

Table 1: Absolute and relative aggregate pathloss gains with relays placed between source and destination separated by 500 m caused by the non-linear propagation model.

2.3 Shadowing Modeling

– Aggregate Shadowing Powergains [1/2] –

- **Decrease of Shadowing Variations.** In the case of serial relays with independent shadowing channels in each relaying hop, the performance is impacted by the weakest relaying segment. Therefore, the decrease in shadowing variation due to shorter communication distances significantly boosts performance of regenerative relaying systems.
- **Example Topology.** Let us again assume a system with the source and destination separated by d meters and relays placed at equidistance between them so that N relay segments occur. Using then e.g. the model of [2], the shadowing standard deviation in each relaying segment can be calculated in decibel as:

$$\sigma_{\text{dB}} = S_s \cdot \left(1 - e^{-\frac{d/N - d_0}{D_s}} \right), \quad (5)$$

where S_s , d_0 and D_s are some model specific constants.

– Aggregate Shadowing Powergains [2/2] –

- Aggregate Shadowing Powergains.** Typically, the power margin due to shadowing is assumed to be about three times its standard deviation σ_{dB} . The aggregate power gains due to this non-linear shadowing behavior, calculated as $10 \log_{10} N + 3\sigma_{\text{dB}}$, is summarized in Table 4 w.r.t. the case without relay in percent and in absolute dB values, assuming $d = 500$ m, $S_s = 22.1$ dB, $d_0 = 10$ m and $D_s = 53$ m.
- General Trends.** These gains are fairly high for a large number of relays but turn into losses for a small number of relays, i.e. in the region of practical deployment. They are due to a small decrease in shadowing standard deviation for large distances and a strong decrease at very short distances.

Relay Segments	1	2	3	4	5	6	7	8	9	10
Relative Gain [%]	0	-3	-2	2	8	15	23	31	39	47
Absolute Gain [dB]	0	-2	-1	2	5	9	12	16	19	21

Table 2: Absolute and relative aggregate shadowing gains.

– Change of Shadow Correlation Model –

- **Change of Shadowing Correlation Model.** In contrast to cellular systems, a cooperative system is composed of transmitting and receiving nodes with similar characteristics in terms of antenna height, etc. The shadowing fluctuations seen by the nodes at both ends of the radio link are therefore statistically identical [3].
- **Novel Correlation Function.** Extensive ray-tracing simulations have revealed that the JCF is well approximated by:

$$R(\Delta d_t, \Delta d_r) \propto e^{-\frac{\Delta d_t + \Delta d_r}{d_{\text{corr}}}}, \quad (6)$$

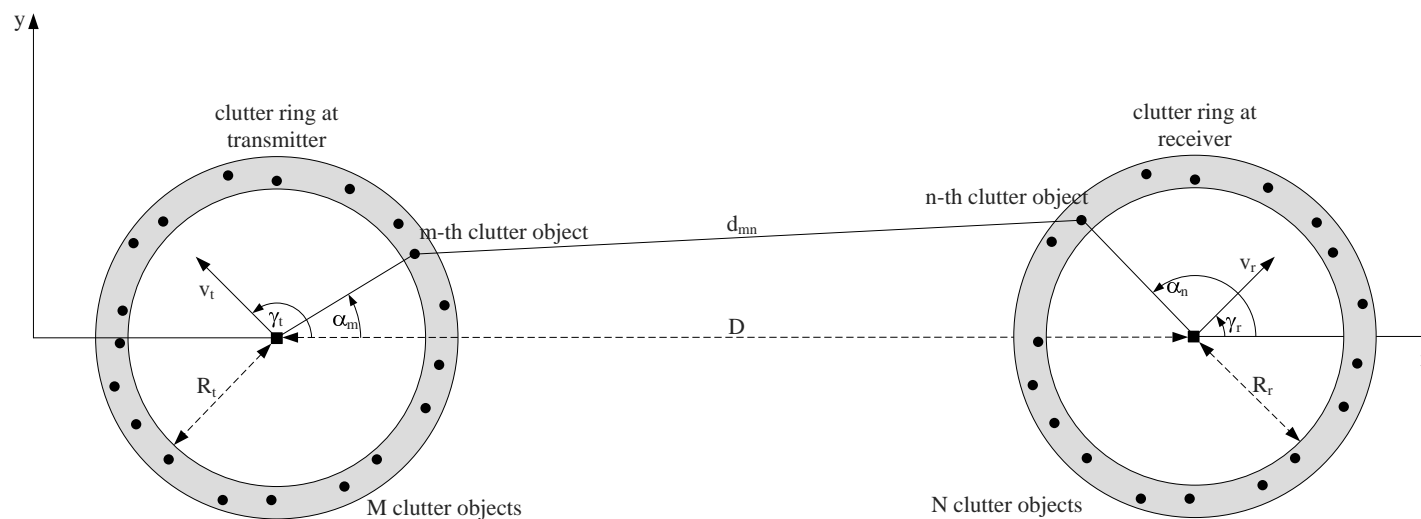
where Δd_t and Δd_r are the displacement distances of the transmitter and receiver, respectively, and d_{corr} the spatial correlation distance.

- **Change in Spatial Correlation Distance.** This spatial correlation distance is often less than observed in cellular systems, where a typical mean value in urban environments is $d_{\text{corr}} = 40$ m [4].

2.4 Fading Modeling

– Geometrical Model –

- **Geometrical Model.** Having originated in [5], this geometrical model is based on the following assumptions:
 - clutter is surrounding transmitter and receiver circularly and uniformly, forming a ring of scatterers;
 - waves which are reflected off several clutter surfaces as well as those which are further away are negligible because they suffer from increased pathloss;
 - the number of scatterers at either end is tending towards infinity, requiring that the power of each wave is negligible compared to the total mean power.



– Baseband Double-Bounced Model –

- **Baseband Model.** The baseband narrowband channel realization can be written as a superposition of any LOS, single bounced (SB) components which have only been bounced at the transmitter (SBT) and only bounced at the receiver (SBR), and the double bounced (DB) components.
- **Double Bounced Component.** Dealing here only with the double bounced component, it can be written as [6]:

$$h^{\text{DB}}(t) = \lim_{M,N \rightarrow \infty} \sum_{m=1}^M \sum_{n=1}^N a_{mn} \cdot e^{j(2\pi f_{mn}t - kd_{mn} + \phi_{mn})}, \quad (7)$$

where a_{mn} and ϕ_{mn} are the joint channel gain and phase shift caused by the interaction of m —th scatterers at the transmitter and n —th scatterer at the receiver; f_{mn} is the Doppler shift induced by moving Tx & Rx; kd_{mn} is the phase shift induced due to the wave traversing a distance d_{mn} whilst traveling from transmitter to receiver.

– Modeling Parameters [1/3] –

- **Modeling Parameters.** These variables are characterized as follows:

- **Amplitude** a_{mn} . The amplitude introduced by the m –th clutter at the transmitter is of the same relative magnitude but independent of the amplitude due to the n –th clutter at the receiver:

$$a_{mn} = a_m \cdot a_n = \frac{1}{\sqrt{MN}}, \quad (8)$$

where the last equation results from normalizing conditions which require that the power of (7) remains bounded and equal to one as $M, N \rightarrow \infty$.

- **Phase** ϕ_{mn} . The phase shift introduced by the m –th clutter at the transmitter is independent of the phase shift introduced by the n –th clutter at the receiver:

$$\phi_{mn} = \phi_m + \phi_n. \quad (9)$$

These phase shifts are random and, since the number of scatterers at either end is approaching infinity, these discrete random variables become continuous with PDFs $p_{\phi_t}(\phi_t)$ and $p_{\phi_r}(\phi_r)$, respectively. It can generally be assumed that they are uniformly distributed.

– Modeling Parameters [2/3] –

- **Modeling Parameters.** ... continued ...

- **Doppler Shift** f_{mn} . The Doppler shifts depend on the geometrical relation between direction of movement of transmitter or receiver and direction of departure or arrival of the wave. The Doppler shift introduced by the m –th clutter at the transmitter is generally independent of the Doppler shift introduced by the n –th clutter at the receiver:

$$f_{mn} = f_m + f_n \quad (10a)$$

$$f_m = \hat{f}_t \cdot \cos(\alpha_m - \gamma_t), \quad (10b)$$

$$f_n = \hat{f}_r \cdot \cos(\alpha_n - \gamma_r), \quad (10c)$$

where \hat{f}_t and \hat{f}_r are respectively the maximum Doppler shifts experienced at the transmitter and receiver and which are given as $\hat{f}_t = f_c \cdot v_t/c = v_t/\lambda$ and $\hat{f}_r = f_c \cdot v_r/c = v_r/\lambda$ with f_c being the carrier frequency and λ the wavelength. Since the location of the scatterers is not known a priori, the AOD α_m and AOA α_n are discrete random variables. However, since the number of scatterers at either end is approaching infinity, these discrete random variables become continuous with PDFs $p_{\alpha_t}(\alpha_t)$ and $p_{\alpha_r}(\alpha_r)$, respectively.

– Modeling Parameters [3/3] –

- **Modeling Parameters.** ... continued ...

- **Path Length** d_{mn} . The path length is impacted by the geometrical arrangement of clutter w.r.t. transmitter and receiver.

Case #1 – D is not significantly larger than $\max(R_t, R_r)$: This is typically encountered indoors and requires the exact expression for d_{mn} to be used:

$$d_{mn} = R_t + \sqrt{(R_t \sin \alpha_m - R_r \sin \alpha_n)^2 + (D - R_t \cos \alpha_m + R_r \cos \alpha_n)^2} + R_r, \quad (11)$$

which essentially prevents one from decoupling the two sums in (7) into two separate sums. Therefore, the CLT applies to the entire expression and the envelope $a = |h|$ is Rayleigh distributed.

Case #2 – $D \gg \max(R_t, R_r)$: It is typically encountered outdoors, leading to [6]:

$$d_{mn} \approx D + R_t \cdot (1 - \cos \alpha_m) + R_r \cdot (1 + \cos \alpha_n), \quad (12)$$

allowing to decouple the two sums in (7) into two separate sums, the resulting envelope being double-Rayleigh.

2.5 Fading Distributions

– Fading Distributions –

- **Unchanged Distributions.** With respect to non-cooperative systems, the statistical distributions of the complex channel, its envelope and power remain generally unchanged (unless there is a cascaded fading channel.)
- **Example Nakagami Distribution.** The PDFs of Nakagami- m envelope and power are:

$$p_a(a) = \frac{2m^m a^{2m-1}}{(\bar{g})^m \Gamma(m)} \exp\left(-\frac{ma^2}{\bar{g}}\right) \quad (13a)$$

$$p_g(g) = \frac{m^m (g)^{m-1}}{(\bar{g})^m \Gamma(m)} \exp\left(-\frac{mg}{\bar{g}}\right), \quad (13b)$$

where $\Gamma(\cdot)$ is the complete Gamma function and m is the Nakagami fading factor. Furthermore, a is the amplitude and g the power. This reduces to the Rayleigh fading case for $m = 1$ and a non-fading channel for $m \rightarrow \infty$. The Gamma distribution is well applicable to all MPCs which suffer from obstructed LOS or weak NLOS conditions.

2.6 Temporal Characteristics

– Temporal Autocorrelation Function [1/3] –

- **Importance.** The temporal ACF of the complex fading channel $h(t)$ is an important quantity since it allows to quantify the required pilot density and interleaver depths for coherent systems, the performance degradation for both coherent as well as non-coherent systems, etc.
- **Definition.** We will henceforth deal with the normalized ACF which is defined as

$$R(\Delta t) = \frac{\mathbb{E} \{h(t + \Delta t) \cdot h^*(t)\}}{\sqrt{\text{VAR} \{h(t + \Delta t)\} \cdot \text{VAR} \{h^*(t)\}}}, \quad (14)$$

where the expectation is taken w.r.t. the set of random variables which in our case are $\alpha_t, \alpha_r, \phi_t$ and ϕ_r . Furthermore, it is henceforth assumed that the average channel power $\text{VAR} \{h(t)\} = 1$ which allows us to drop it in subsequent derivations.

– Temporal Autocorrelation Function [2/3] –

- **ACF for M2M.** We can calculate the ACF as follows:

$$R(\Delta t) = \mathbb{E} \left\{ \lim_{M, N \rightarrow \infty} \sum_{m=1}^M \sum_{n=1}^N \frac{1}{\sqrt{MN}} \cdot e^{j(2\pi(f_m + f_n)(t + \Delta t) + kd_{mn} + \phi_m + \phi_n)} \times \right. \\ \left. \lim_{M, N \rightarrow \infty} \sum_{m'=1}^M \sum_{n'=1}^N \frac{1}{\sqrt{MN}} \cdot e^{-j(2\pi(f_{m'} + f_{n'})t + kd_{m'n'} + \phi_{m'} + \phi_{n'})} \right\} \quad (15a)$$

$$= \int_{-\pi}^{\pi} e^{j2\pi \hat{f}_t \cdot \cos(\alpha_t - \gamma_t) \Delta t} p_{\alpha_t}(\alpha_t) d\phi_t \times \\ \int_{-\pi}^{\pi} e^{j2\pi \hat{f}_r \cdot \cos(\alpha_r - \gamma_r) \Delta t} p_{\alpha_r}(\phi_r) d\phi_r \quad (15b)$$

$$= J_0 \left(2\pi \hat{f}_t \Delta t \right) \cdot J_0 \left(2\pi \hat{f}_r \Delta t \right), \quad (15c)$$

where $J_0(\cdot)$ is the zeroth order Bessel function of the first kind.

– Temporal Autocorrelation Function [3/3] –

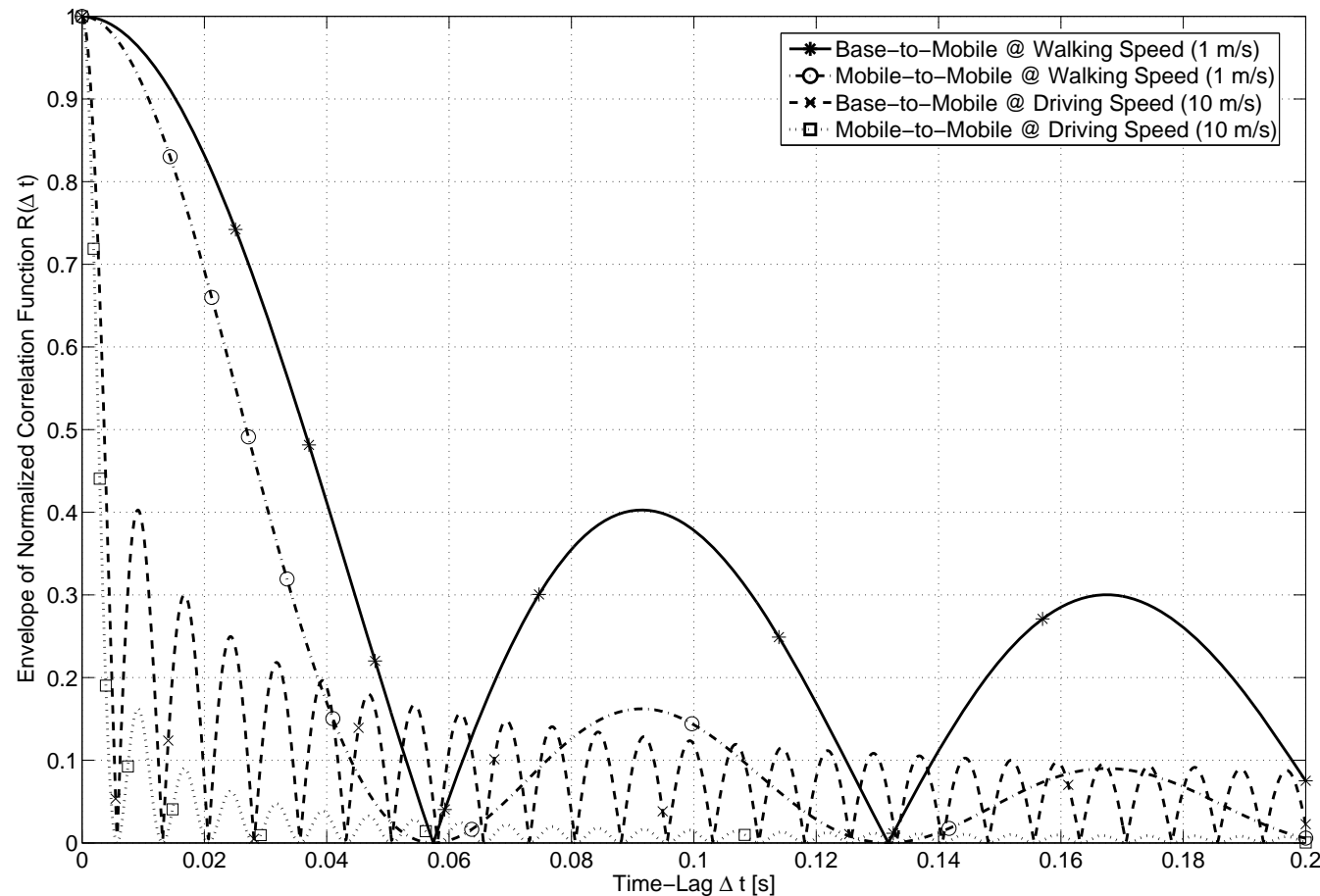


Figure 8: Absolute value of the temporal autocorrelation function of the complex fading channel for the base-to-mobile and mobile-to-mobile scenarios at $f_c = 2$ GHz. Observations: MS-to-MS channel decorrelates faster than BS-to-MS channel; good for code design, bad for channel estimation.

– Doppler Power Spectrum –

- **Definition.** The Doppler power spectrum of the complex channel $h(t)$ is determined from the Fourier transform of its temporal autocorrelation function $R(\Delta t)$, i.e.

$$\Psi(f) = \int_{-\infty}^{\infty} R(\Delta t) e^{-j2\pi f \Delta t} d\Delta t. \quad (16)$$

This transformation does clearly not yield any novel insights w.r.t. the already available autocorrelation function. However, it is of great value when simulating fading channels.

- **Doppler of M2M Channel.** Applying the Fourier transform to (15c) yields [7]:

$$\Psi(f) = \frac{1}{\pi^2 \sqrt{\hat{f}_t \hat{f}_r}} K \left[\sqrt{\frac{(\hat{f}_t + \hat{f}_r)^2 - f^2}{4\hat{f}_t \hat{f}_r}} \right], \quad (17)$$

where $K(\cdot)$ is the complete elliptic integral of the first kind. This function exhibits two peaks at $\pm(\hat{f}_t - \hat{f}_r)$ and is generally symmetric w.r.t. the motion of Tx/Rx.

– Level Crossing Rate –

- **Definition.** The level crossing rate of the channel's envelope represents the expected number of times per second the channel amplitude $a = |h|$ crosses level a_{thr} in the positive direction. It is an important notion for adaptive or opportunistic systems in that it quantifies the frequency the channel state changes and hence the frequency for need of adaptation or opportunity.
- **LCR of M2M Channel.** It can be calculated as [8]:

$$N(a_{\text{thr}}) = \sqrt{2\pi \left(\hat{f}_t^2 + \hat{f}_r^2 \right)} \cdot a_{\text{thr}} \cdot e^{-a_{\text{thr}}^2}, \quad (18)$$

assuming that $\mathbb{E} \{ |h|^2 \} = 1$. Generally, the MS-to-MS channel varies faster than BS-to-MS channel, which is advantageous since it creates opportunities more frequently but requires also more frequent adaptations, e.g. change of modulation and coding scheme.

– Average Fade Duration –

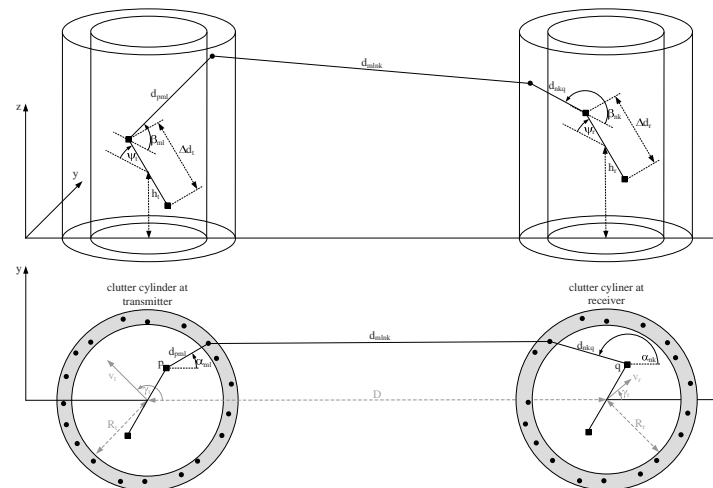
- **Definition.** It is the average duration of time the envelope spends below level a_{thr} . Again, it is an important notion for adaptive or opportunistic systems in that it quantifies the duration the system remains in the same state, e.g. same modulation order, etc.
- **AFD of M2M Channel.** It can be calculated as:

$$T(a_{\text{thr}}) = \frac{1}{\sqrt{2\pi (\hat{f}_t^2 + \hat{f}_r^2)}} \left(e^{a_{\text{thr}}^2} - 1 \right). \quad (19)$$

Again, the AFD of mobile-to-mobile channels is generally lower than of base-to-mobile channels due to the higher mobility at either end.

– Advanced Modeling –

- **Advanced Modeling.** Following exactly the same approach but with a little more involved mathematics, one can derive the temporal, spatial and spectral characteristics of the following cases:
 - Non-Isotropic Scattering Scenario
 - Ricean Fading Scenario
 - MIMO System
 - 3D Clutter Distribution
- **Spectral-Spatial-Temporal Characteristics.** An example model is:



PART 3

Transparent Relaying Channel

3.1 Quick Intro

– Typical Transparent Topology –

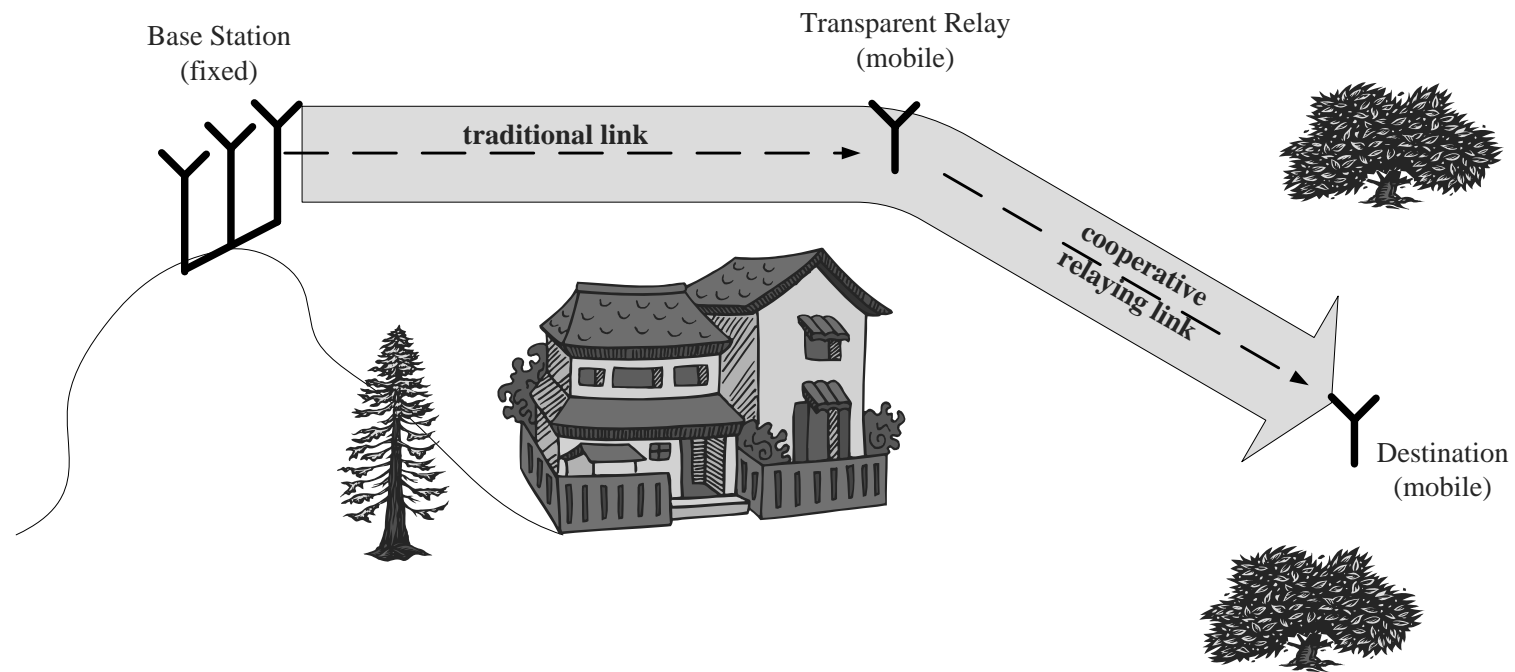


Figure 9: An example of a transparent relaying channel.

– System Assumption [1/2] –

- **Coupling of Relay Stages.** Transparent relaying couples the fading channels and the topology hence becomes part of the channel.
- **Modeling Approach.** In the example case of one relay leading to two relaying segments, the effective received signal is given as:

$$y_2 = \sqrt{G_2} \cdot h_2 \cdot A \cdot y_1 + n_2 \quad (20a)$$

$$y_1 = \sqrt{G_1} \cdot h_1 \cdot x_1 + n_1 \quad (20b)$$

which can be rewritten as

$$y_2 = A \cdot \sqrt{G_1 G_2} \cdot h_1 h_2 \cdot x_1 + A \cdot \sqrt{G_2} \cdot h_2 \cdot n_1 + n_2, \quad (21)$$

where the end-to-end wireless channel is characterized by $A \cdot \sqrt{G_1 G_2} h_1 h_2$ and the additive noise by $A \cdot \sqrt{G_2} \cdot h_2 \cdot n_1 + n_2$.

– System Assumption [2/2] –

- **Amplification Factor.** A is the amplification factor which can generally be variable, averaged or fixed:
 - **Variable Amplification Factor.** Relay has knowledge on the instantaneous fading conditions of the source to relay channel and the amplification factor counterweights deep fades:

$$A = \sqrt{\frac{P_2}{P_1 g_1 + \sigma_1^2}}, \quad (22)$$

where P_1 and P_2 are the respective average transmission powers of the sender and relay, g_1 is the instantaneous channel power in the first relaying segment and σ_1^2 is AWGN.

- **Average Amplification Factor.** The amplification in the relay injects in average the same power as the amplification given in (22), which yields the condition [9]:

$$A = \sqrt{\mathbb{E} \left\{ \frac{P_2}{P_1 g_1 + \sigma_1^2} \right\}}, \quad (23)$$

Different relaying channel statistics hence require very different amplifications.

– Impact on End-to-End Performance –

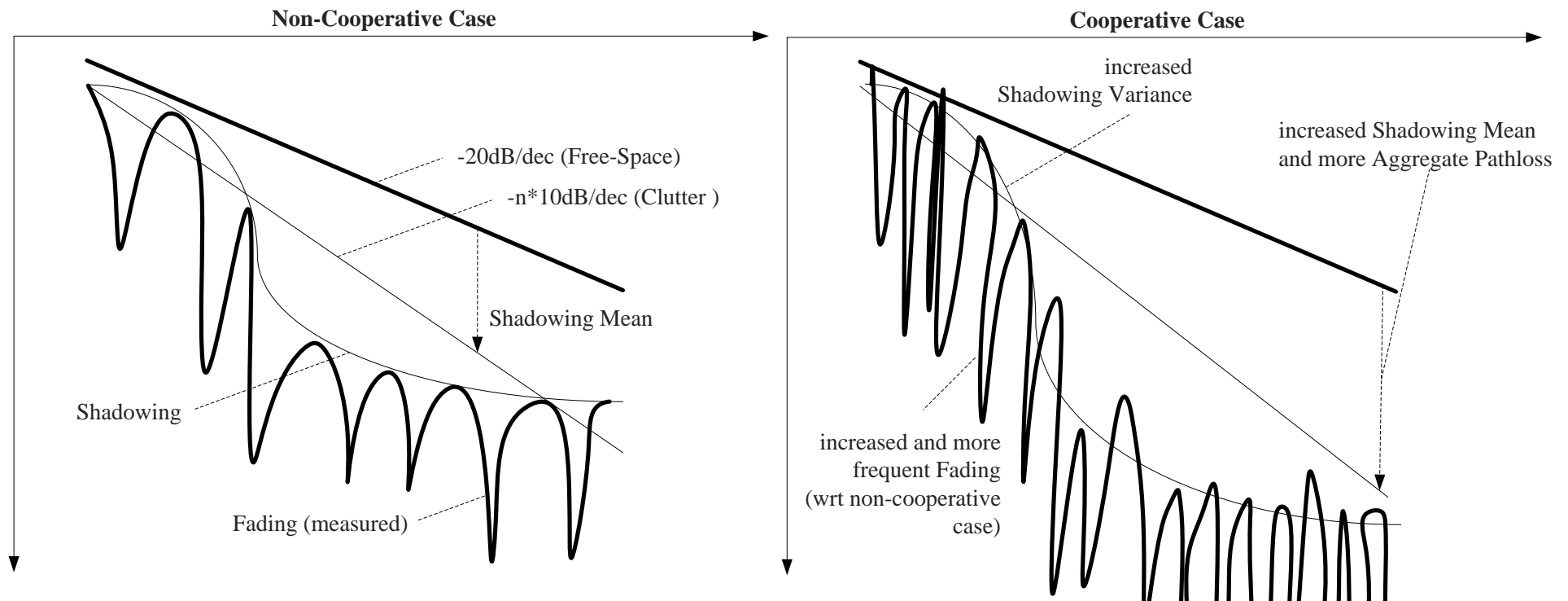
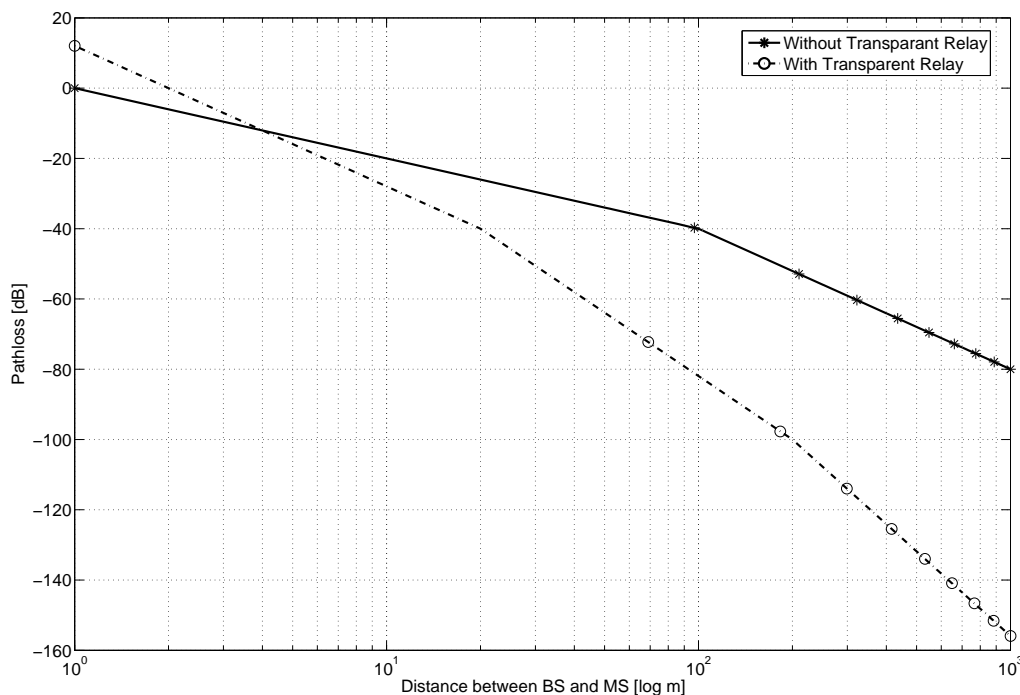


Figure 10: Transparent cooperative communication worsens fading behavior and also impacts shadowing and pathloss.

3.2 Pathloss Modeling

– Change of Breakpoint Behavior –

- **Change of Breakpoint Behavior.** The lower antenna heights together with the coupling of the relaying segments, yields fairly complex pathloss behaviors which can be quantified for a given pathloss model at hand.
- **Example Behavior.** Comparison between cases of no relay with fixed-gain relay placed exactly between transmitter and receiver.



– Increased Pathloss [1/2] –

- **Per-Stage Pathloss.** Let us assume for simplicity e.g. a fixed amplification factor and a single-slope pathloss model for both relaying stages. It is of the form

$L_i(d) = b_i + n_i \log_{10}(d)$, where b_i is some normalization constant and n_i the pathloss coefficient.

- **End-to-End Pathloss.** It can be written as the sum of each segment's contribution, i.e. $b_1 + b_2 + n_1 \log_{10}(d_1) + n_2 \log_{10}(d_2)$, where $d = d_1 + d_2$. If the transparent relay is placed exactly midway between transmitter and receiver and both relaying segments exhibit the same pathloss behavior, this expression simplifies to $2b + 2n \log_{10}(d/2)$. The end-to-end pathloss hence experiences a change in parameters, i.e.

$$L(d) = b' + n' \log_{10}(d) \quad (24)$$

where $b' = 2b - 2n \log_{10} 2$ and $n' = 2n$. This leads to an increased pathloss slope and shift as already observed in the previous figure.

– Increased Pathloss [2/2] –

- **Example Pathloss Calculation.** To quantify this loss for an arbitrary number of relaying segments, let us e.g. assume a system with the source and destination separated by $d = 500$ m and relays placed at equidistance between them so that N relay segments occur. Then, with the model of [2], we have $b = -62.01$ dB and $n = 5.86$ leading to $b' = -62.01 \cdot N - 5.86 \cdot \log_{10} N$ dB and $n = 5.86 \cdot N$.
- **General Trends.** These losses diminish with variable amplification factor but are generally very large.

Relay Segments	1	2	3	4	5	6	7	8	9	10
Relative Gain [%]	0	-50	-66	-75	-80	-83	-86	-87	-89	-90

Table 3: Absolute and relative pathloss losses with relays placed between source and destination separated by 500 m caused by the non-linear propagation model.

3.3 Shadowing Modeling

– Aggregate Shadowing Powerlosses [1/2] –

- **Increase of Shadowing Variations.** In the case of transparent relays with independent shadowing channels in each relaying segment, the aggregated shadowing still obeys a Gaussian distribution in decibels, however, with a changed standard deviation w.r.t. a direct link. Using (21), the effective end-to-end shadowing standard deviation with N transparent relaying segments and a fixed amplification factor is given as

$$\sigma_{e2e,dB} = \sqrt{N} \sigma_{dB}.$$

- **More Realistic Model.** Using a more sophisticated model, such as given in [2], the aggregated end-to-end shadowing standard deviation for N equally long relaying segments can be calculated in decibel as follows:

$$\sigma_{e2e,dB} = \sqrt{N} \cdot S_s \cdot \left(1 - e^{-\frac{d/N - d_0}{D_s}} \right), \quad (25)$$

where S_s , d_0 and D_s are some model specific constants and d is the distance between source and destination.

– Aggregate Shadowing Powerlosses [2/2] –

- **Example Model Realization.** The increase in shadowing standard deviation w.r.t. the case without relay in percent and in absolute dB values is summarized in Table 4, assuming $d = 500$ m, $S_s = 22.1$ dB, $d_0 = 10$ m and $D_s = 53$ m.
- **General Trends.** These losses are generally not negligible and further aggravate above discussed pathlosses. It is interesting to observe however that with above model, the shadowing losses start to diminish after around 5 relays and even turn into gains beyond 20 relays (not shown). This is due to a strong decrease of the shadowing standard deviation at very short distances.

Relay Segments	1	2	3	4	5	6	7	8	9	10
Relative Gain [%]	0	-29	-39	-44	-45	-46	-45	-44	-42	-40
Absolute Gain [dB]	0	-9	-14	-17	-18	-18	-18	-17	-16	-15

Table 4: Absolute and relative aggregate shadowing losses with relays placed between source and destination separated by 500 m caused by the non-linear behavior of the shadow standard deviation.

– Change of Shadow Correlation Model –

- **Absence of Correlation Models.** There are no rigorously derived or measured models yet available for the JCF in the context of transparent relaying systems.
- **Proposed Correlation Function.** However, based on [3] and some parallels drawn from the temporal correlation function of transparent relay channels:

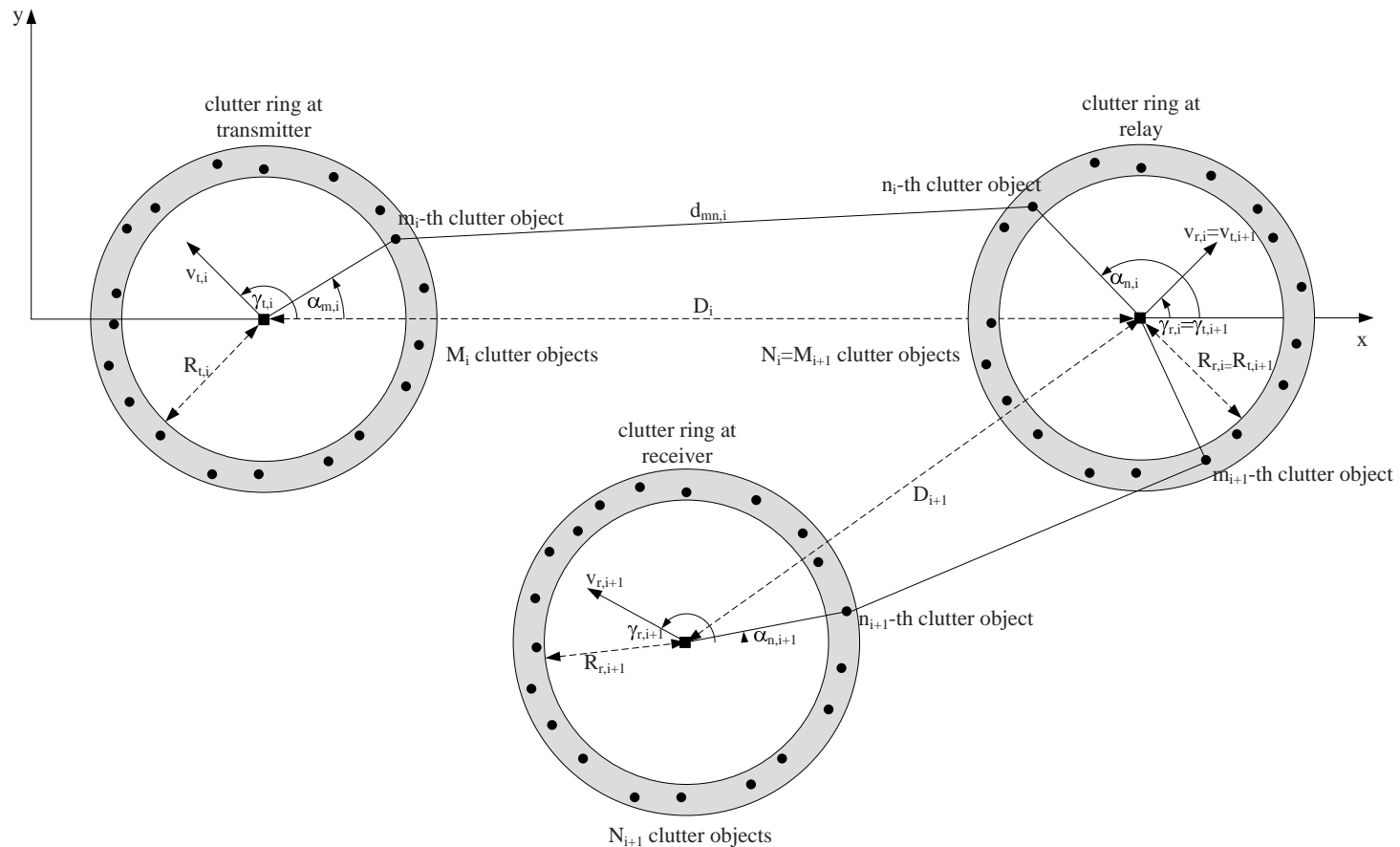
$$R(\Delta d_{t1}, \Delta d_{r1}, \Delta d_{t2}, \Delta d_{r2}) \propto e^{-\frac{\Delta d_{t1} + \Delta d_{r1}}{d_{\text{corr1}}}} \cdot e^{-\frac{\Delta d_{t2} + \Delta d_{r2}}{d_{\text{corr2}}}}, \quad (26)$$

where Δd_{t1} , Δd_r and $\Delta d_{r1} = \Delta d_{t2}$ are the displacement distances of the transmitter, receiver and relay, respectively. Furthermore, d_{corr1} and d_{corr2} are the spatial correlation distance observed in the first and second relaying segment. This expression is dominated by the term with the smaller correlation distance.

3.4 Fading Modeling

– Geometrical Model –

- Geometrical Model.** Following the approach as for the regenerative channel, this geometrical model is based on the same assumptions.



– Baseband Double-Bounced Model –

- **Baseband Model.** The baseband narrowband channel realization can be written as a superposition of any LOS, SBT, SBR and DB components.
- **Double Bounced (BD) Component.** Dealing here only with the double bounced component, it can be written as [6]:

$$h(t) = \prod_{i=1}^N h_i = \prod_{i=1}^N h_i^{\text{DB}} \quad (27)$$

$$= \prod_{i=1}^N \lim_{M_i, N_i \rightarrow \infty} \sum_{m_i=1}^{M_i} \sum_{n_i=1}^{N_i} \frac{1}{\sqrt{M_i N_i}} \cdot e^{j(2\pi(f_{m,i} + f_{n,i})t - kd_{mn,i} + \phi_{m,i} + \phi_{n,i})} \quad (28)$$

where i relates to the relaying segment and generally the same notation as for the regenerative channel has been used.

3.5 Fading Distributions

– Constant Amplification Factor–

- Cascaded Rayleigh Fading.** The double-Rayleigh channel results from the product of two complex Gaussian processes, i.e. $h = h_1 \cdot h_2$, the amplitude/envelope of which is $a = |h| = |h_1| \cdot |h_2| = a_1 \cdot a_2$ and the gain/power of which is $g = |h|^2 = |h_1|^2 \cdot |h_2|^2 = g_1 \cdot g_2$.
- Resultant PDF.** Using the rule for the PDF transformations of products of random variables, one easily establishes that the resultant PDF is given as:

$$p_g(g) = \int_0^{\infty} \frac{1}{A^2 \xi} \cdot p_{g_1}(\xi) \cdot p_{g_2}\left(\frac{g}{A^2 \xi}\right) d\xi \quad (29a)$$

$$= \int_0^{\infty} \frac{1}{A^2 \xi} \cdot \frac{1}{\bar{g}_1} \exp\left(-\frac{\xi}{\bar{g}_1}\right) \cdot \frac{1}{\bar{g}_2} \exp\left(-\frac{g}{\bar{g}_2 A^2 \xi}\right) d\xi \quad (29b)$$

$$= \frac{1}{A^2} \frac{2}{\bar{g}_1 \cdot \bar{g}_2} \cdot K_0\left(2\sqrt{\frac{1}{A^2} \frac{g}{\bar{g}_1 \cdot \bar{g}_2}}\right), \quad (29c)$$

where $K_0(\cdot)$ is the zeroth order modified Bessel function of the second kind.

– Variable Amplification Factor–

- **Transposition of Problem.** The power of the end-to-end transparent relay channel with variable amplification, i.e.

$$g = \frac{P_2}{P_1} \cdot \frac{g_1 g_2}{g_1 + \sigma_1^2 / P_1} \quad (30)$$

is in structure the same as the end-to-end SNR in transparent relay channels with constant amplification. This allows one to reuse prior tools and results.

- **Resultant PDF.** The PDF of the channel power e.g. is given as:

$$p_g(g) = \frac{2P_1}{P_2 \bar{g}_2} e^{-\frac{P_1 g}{P_2 \bar{g}_2}} \quad (31a)$$

$$\times \left(\sqrt{\frac{\sigma_1^2 g}{P_2 \bar{g}_1 \bar{g}_2}} K_1 \left[2 \sqrt{\frac{\sigma_1^2 g}{P_2 \bar{g}_1 \bar{g}_2}} \right] + \frac{\sigma_1^2}{P_1 \bar{g}_1} K_0 \left[2 \sqrt{\frac{\sigma_1^2 g}{P_2 \bar{g}_1 \bar{g}_2}} \right] \right) .$$

3.6 Temporal Characteristics

– ACF for Constant Amplification –

- **Cascaded Channel.** The first to report on the ACF of the transparent relaying channel was [10], which used the fact that the channel is of the form $h = h_1 h_2$ where h_1 and h_2 are respectively the channels of the first and second relaying segments.
- **Resultant ACF.** Assuming a constant amplification factor A , the normalized ACF can be calculate as [10]:

$$R(\Delta t) = \mathbb{E} \{h(t + \Delta t) \cdot h^*(t)\} \quad (32a)$$

$$= \mathbb{E} \{h_1(t + \Delta t)h_1^*(t)h_2(t + \Delta t)h_2^*(t)\} \quad (32b)$$

$$= R_1(\Delta t) \cdot R_2(\Delta t) \quad (32c)$$

$$= \prod_{i=1}^2 J_0 \left(2\pi \hat{f}_{t,i} \Delta t \right) \cdot J_0 \left(2\pi \hat{f}_{r,i} \Delta t \right) . \quad (32d)$$

– ACF for Variable Amplification –

- **Approximation.** With variable amplification and a high operational SNR allows the end-to-end channel to be approximated by $h(t) \approx \sqrt{P_2/P_1} \exp[j\theta_1(t)] \cdot h_2(t)$.
- **Resultant ACF.** The normalized ACF can be calculated as [10]:

$$R(\Delta t) \approx \mathbb{E} \{ \exp[j\theta_1(t + \Delta t)] \exp[-j\theta_1(t)] h_2(t + \Delta t) h_2^*(t) \} \quad (33a)$$

$$= J_0 \left(2\pi \hat{f}_{t,1} \Delta t \right) \left[1 - J_0^2 \left(2\pi \hat{f}_{t,1} \Delta t \right) \right] \quad (33b)$$

$$\times {}_2F_1 \left(\frac{3}{2}, \frac{3}{2}, 2, J_0^2 \left(2\pi \hat{f}_{t,1} \Delta t \right) \right)$$

$$J_0 \left(2\pi \hat{f}_{r,1} \Delta t \right) \left[1 - J_0^2 \left(2\pi \hat{f}_{r,1} \Delta t \right) \right]$$

$$\times {}_2F_1 \left(\frac{3}{2}, \frac{3}{2}, 2, J_0^2 \left(2\pi \hat{f}_{r,1} \Delta t \right) \right)$$

$$\times J_0 \left(2\pi \hat{f}_{t,2} \Delta t \right) \cdot J_0 \left(2\pi \hat{f}_{r,2} \Delta t \right) .$$

4. Concluding Remarks

– Transparent Relaying Channel –

- **Peculiarities.** Applicable to transparent relaying protocols, such as the AF protocol, this channel has the following peculiarities:
 - Despite the reduced communication distances and hence generally less pathloss and shadowing per relaying stage, the transparent nature of the system amplifies the breakpoint behavior, augments the shadowing variations and typically increases the end-to-end delay spread.
 - Due to mobile transmitter and mobile receiver, the temporal correlation is greatly impacted, generally yielding deeper and more frequent fades.
 - Due to the transparent nature of the system, all relaying segments are coupled making fading behavior dependent on the system topology and leading to novel amplitude statistics of more severe behavior.
- **Verdict.** The major part of the performance loss in transparent relaying systems originates indisputably from the aggravation of the statistical variations of each relaying segment, be they due to shadowing or fading.

– Regenerative Relaying Channel –

- **Peculiarities.** Applicable to regenerative relaying protocols, such as the DF protocol, this channel has the following peculiarities:
 - The reduced communication distances yield generally less aggregated pathloss, less aggregated shadowing variations and shorter delay spreads and hence a significant reduction in frequency selectivity.
 - Due to mobile transmitter and mobile receiver, the temporal correlation is greatly impacted, mainly yielding more frequent fades.
 - Due to the regenerative nature of the system, each relaying segment is decoupled leading to the observation of known amplitude statistics.
- **Verdict.** The major part of the performance gains in regenerative relaying systems originates indisputably from pathloss and to some extent shadowing gains but not from fading gains.

References

- [1] A. Matveev, *Electrodynamics and Relativity Theory*. Moscow Press, in Russian, 1964.

- [2] Z. Wang, E. K. Tameh, and A. R. Nix, "Statistical peer-to-peer channel models for outdoor urban environments at 2 GHz and 5 GHz," in *Vehicular Technology Conference, 2004. VTC2004-Fall. 2004 IEEE 60th*, vol. 7, pp. 5101–5105, Sept. 26–29, 2004.

- [3] Z. Wang, E. K. Tameh, and A. R. Nix, "Joint Shadowing Process in Urban Peer-to-peer Radio Channels," *IEEE Transactions on Vehicular Technology*, vol. 57, pp. 52–64, Jan. 2008.

- [4] K. Konstantinou, S. Kang, and C. Tzaras, "A Measurement-based Model for Mobile-to-mobile UMTS Links," in *Vehicular Technology Conference, 2007. VTC2007-Spring. IEEE 65th*, (Dublin), pp. 529–533, Apr. 22–25, 2007.

- [5] G. J. Byers and F. Takawira, "Spatially and temporally correlated MIMO channels: modeling and capacity analysis," *IEEE Transactions on Vehicular Technology*, vol. 53, pp. 634–643, May 2004.

- [6] M. Patzold, B. O. Hogstad, and N. Youssef, "Modeling, analysis, and simulation of MIMO mobile-to-mobile fading channels," *IEEE Transactions on Wireless Communications*, vol. 7, pp. 510–520, Feb. 2008.

REFERENCES

- [7] A. S. Akki and F. Haber, "A statistical model of mobile-to-mobile land communication channel," *IEEE Transactions on Vehicular Technology*, vol. 35, pp. 2–7, Feb. 1986.

- [8] A. S. Akki, "Statistical properties of mobile-to-mobile land communication channels," *IEEE Transactions on Vehicular Technology*, vol. 43, pp. 826–831, Nov. 1994.

- [9] M. O. Hasna and M. S. Alouini, "A performance study of dual-hop transmissions with fixed gain relays," *IEEE Transactions on Wireless Communications*, vol. 3, pp. 1963–1968, Nov. 2004.

- [10] C. S. Patel, G. L. Stuber, and T. G. Pratt, "Statistical properties of amplify and forward relay fading channels," *IEEE Transactions on Vehicular Technology*, vol. 55, pp. 1–9, Jan. 2006.